

Differentiable Constrained Imitation Learning for Robot Motion Planning and Control

Christopher Diehl, Janis Adamek, Martin Krüger, Frank Hoffmann and Torsten Bertram

Abstract—Motion planning and control are crucial components of robotics applications. Here, spatio-temporal hard constraints like system dynamics and safety boundaries (e.g., obstacles in automated driving) restrict the robot’s motions. Direct methods from optimal control solve a constrained optimization problem. However, in many applications finding a proper cost function is inherently difficult because of the weighting of partially conflicting objectives. On the other hand, Imitation Learning (IL) methods such as Behavior Cloning (BC) provide a intuitive framework for learning decision-making from offline demonstrations and constitute a promising avenue for planning and control in complex robot applications. Prior work primarily relied on soft-constraint approaches, which use additional auxiliary loss terms describing the constraints. However, catastrophic safety-critical failures might occur in out-of-distribution (OOD) scenarios. This work integrates the flexibility of IL with hard constraint handling in optimal control. Our approach constitutes a general framework for constraint robotic motion planning and control using offline IL. Hard constraints are integrated into the learning problem in a differentiable manner, via explicit completion and gradient-based correction. Simulated experiments of mobile robot navigation and automated driving provide evidence for the performance of the proposed method.

I. INTRODUCTION

The motion of robots (e.g., robotic manipulators, mobile robots and self-driving vehicles) in the real world is constrained by the kinematics and dynamics of the robot as well as the geometric structure of the environment. A core challenge is incorporating these constraints into robot planning and control. On the one side, optimal control approaches solve a finite horizon optimal control problem by optimizing a cost function under *explicitly* defined constraints. A common approach, like in direct methods [1], is to derive a nonlinear program from a continuous optimal control formulation [2], [3], [4] and then solve the problem with numerical optimization. However, designing a general cost function remains an unsolved problem for inherently complex tasks such as automated driving [5], [6]. Here, aspects like comfort and safety must be weighed against each other. On the other side, robot behavior can be learned from demonstrations, which is the task of IL. One example is BC, a simple *offline* learning method, requiring no *on-policy* environment interactions. Here, constraints are *implicitly* learned from data. Further, constraints can be integrated by auxiliary loss functions. However, there are

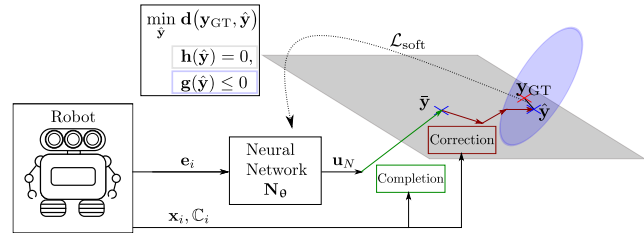


Fig. 1: A schematic overview of the proposed framework: A robot perceives its environment and builds a high-dimensional environment model e_i and a low-dimensional state representation x_i . Constraints C_i further bound the robots motion. A neural network N_θ processes e_i and outputs an initial sequence of control values u_N . These are *completed* to the initial solution \bar{y} , also containing the predicted states, by unrolling a robot dynamics model. Afterward, \bar{y} is *corrected* considering the constraints C_i . The result is an estimated solution \hat{y} , containing a sequence of future states and controls. During training, the framework computes a distance measure between the \hat{y} and the ground truth y_{GT} and backpropagates the softloss \mathcal{L}_{soft} . During testing, the approach delivers a solution that imitates the expert behavior, while obeying a set of nonlinear constraints.

no guarantees for constraint satisfaction, and robot policies fail under distribution shifts [7], causing unexpected unsafe actions.

That raises the question: *Can we combine offline IL methods like BC with the constraint incorporation of optimal control methods?*

Donti et al. [8] present a method for incorporating hard constraints into the training of neural networks. The problem is formulated as a nonlinear program, and evaluated with a simple network architecture. Our approach extends their previous work to the robotic IL setting. The nonlinear program is constructed via direct transcription. Our proposed approach, summarized in Fig. 1, leverages two differentiable procedures to account for equality and inequality constraints and is agnostic to the used network architecture. First, the network predicts a sequence of control vectors, which are explicitly completed to a sequence of states w.r.t. the system dynamics represented as equality constraints. Then, a gradient-based correction accounts for inequality constraints while satisfying the equality constraints.

Contributions. To summarize, the paper makes the following contributions: (i) It proposes a general Differentiable Constraint Imitation Learning (DCIL) framework for incorporating constraints, which is agnostic to the particular neural

This research was funded by the Federal Ministry for Economic Affairs and Energy on the basis of a decision by the German Bundestag in the project “KISSaF - AI-based Situation Interpretation for Automated Driving”.

The authors are with the Institute of Control Theory and Systems Engineering, TU Dortmund University, D-44227, Germany.

network architecture. (ii) It demonstrates the approach’s effectiveness in one mobile robot and one automated driving environment during closed-loop evaluation. The approach outperforms multiple state-of-the art baselines considering a variety of metrics.

II. RELATED WORK

The proposed approach is situated within the broader scope on the integration of constraints into learning-based approaches and IL in the robotics and automated driving literature. This section classifies related work into two major categories.

Modification of the Training Loss. The first class of approaches incorporates constraints by modifying the training loss. A simple approach adds the constraints as weighted penalties to the imitation loss. [9] proposes an application for automated driving. The work shows that additional loss functions penalizing constraint violations improve the closed-loop performance. [10] modifies the training process with a primal-dual formulation and converts the constrained optimization problem into an alternating min-max optimization with Lagrangian variables. [11] uses an energy-based formulation. During training, the loss pushes down the energy of positive samples (close to the expert demonstration) and pulls up the energy-values on negative samples, which violate constraints (e.g., colliding trajectories). While these methods are more robust to errors in constraint-specifications, they often fail in OOD scenarios.

Projection onto Feasible Sets. The second group of approaches projects the neural network’s output onto a solution that is compliant with the constraints. Instead of predicting a future sequence of states, a neural network predicts a sequence of controls [12]. Unrolling a dynamics model generates a feasible state trajectory consistent with the robot system dynamics. However, the approach does not account for general nonlinear inequality constraints. [13] presents an inverse reinforcement learning approach. First, a set of safe trajectories is sampled, and learning is only performed on the safe samples. SafetyNet [14] trains an IL planner and proposes a sampling-based fallback layer performing sanity checks. [15] propose a similar approach using quadratic optimization. Other works incorporate quadratic programs [16] or convex optimization programs [17] as an implicit layer into neural network architectures. These approaches constitute the last layer to project the output to a set of feasible solutions. [18] directly modifies the network architecture by encoding convex polytopes. Sampling, quadratic optimization and convexity severely restrict the solution space.

Most closely related to our approach is the work of [8]. The authors present a hybrid approach, which accounts for nonconvex, nonlinear constraints. Experiments deal with numerical examples with simple network architectures. We extend this work to the real-world-oriented robot IL setting with more complex architectures for high-dimensional feature space. Further, we use an explicit completion by unrolling a robot dynamics model.

Just recently, concurrent works propose approaches which also incorporate nonlinear constraints using Signal Temporal Logic [19] and differentiable control barrier functions [20]. In contrast, our approach relies on a differentiable completion, and gradient-based correction procedure, and the training is guided by auxiliary losses. [19] evaluates on simple toy examples, whereas our analysis considers a more realistic environment. [20] evaluates in real-world experiments but only use a circular robot footprint and object representation, whereas this work evaluates using different constraints. Our approach is able to resolve incorrect constraints that render the problem infeasible. [19] and [20] further emphasize the importance of incorporating nonlinear constraints.

III. PROBLEM FORMULATION

Assume robots dynamics described by nonlinear, time-invariant differential equations with time $t \in \mathbb{R}$, state $\mathbf{x} \in \mathcal{X}$ and controls $\mathbf{u} \in \mathcal{U} \subset \mathbb{R}^{n_u}$:

$$\dot{\mathbf{x}}(t) = \mathbf{f}(\mathbf{x}(t), \mathbf{u}(t)). \quad (1)$$

The state space size \mathcal{X} of dimension n_x is the union of an arbitrary number of real spaces and non-Euclidean rotation groups $\text{SO}(2)$. In addition to the low-dimensional state representation \mathbf{x} , assume access to a high-dimensional environment representation $\mathbf{e} \in E \subset \mathbb{R}^{n_e}$ (e.g., a birds-eye-view (BEV) image of the scene). Further, the system is bounded by a set of nonlinear constraints \mathbb{C} (e.g., by control bounds, rules, or safety constraints).

A (sub-)optimal expert, pursuing a policy π_{exp} , controls the robot and generates a dataset $\mathcal{D} = \{(\mathbf{x}_i, \mathbf{u}_i, \mathbf{e}_i, \mathbb{C}_i)\}_{i=1}^I$ with $I \in \mathbb{N}^+$ samples. A future trajectory of length $H \in \mathbb{N}^+$ containing states and controls belonging to sample i is given by $\mathbf{y}_{\text{GT}} = [\mathbf{x}_i^T, \mathbf{u}_i^T \dots, \mathbf{x}_{i+H}^T, \mathbf{u}_{i+H-1}^T]^T$. During training, the objective is to find the optimal parameters $\theta \in \mathbb{R}^{n_\theta}$ under a maximum likelihood estimation:

$$\theta^* = \arg \min_{\theta} \mathbb{E} [\mathbf{d}(\mathbf{y}_{\text{GT}}, \hat{\mathbf{y}})], \quad (2)$$

subject to equation (1) and the constraints \mathbb{C} . The function \mathbf{d} denotes a distance measure and $\hat{\mathbf{y}} = \pi_{\theta}(\mathbf{x}_i, \mathbf{e}_i)$ is the output of the function π_{θ} parameterized by θ . Function π_{θ} is described by a neural network \mathbf{N}_{θ} and the completion $\mathbf{f}_{\text{compl}}$ and correction \mathbf{f}_{corr} procedure. During inference, given the environment representation, the robot’s goal is to predict a sequence of states and controls compliant with the constraints. In the spirit of an model predictive control (MPC) framework, the first control vector is applied or an underlying tracking controller regulates the robot along the predicted reference.

IV. CONSTRAINED IMITATION LEARNING SYNTHESIS

This section introduces the constrained IL framework. We first show how to construct a nonlinear program per sample used for training the network. Afterwards, the solution process is detailed. A general description of the approach is visualized in Fig. 1.

A. Nonlinear Program Formulation

Direct transcription (see for example [1]) transforms the time-continuous formulation of the constraints \mathbb{C} and equation (1) into a nonlinear program per sample. We discretize¹ the time interval $[t_i, t_{i+H}]$ with $t_i = t_0 \leq t_1 \leq \dots \leq t_k \leq \dots \leq t_H = t_{i+H}$ and $k = 0, 1, \dots, H$. We assume a piecewise constant control $\mathbf{u}(t) := \mathbf{u}_k = \text{constant}$ for $t \in [t_k, t_k + \Delta t)$, where $\Delta t = t_{k+1} - t_k$ for $k = 0, 1, \dots, H-1$ denotes the time interval. The states at grid points t_k are described by $\mathbf{x}(t_k) := \mathbf{x}_k$ for $k = 0, 1, \dots, H$. The forward differences

$$\mathbf{x}_{k+1} = \mathbf{f}(\mathbf{x}_k, \mathbf{u}_k) \quad (3)$$

impose a set of equality constraints $\mathbf{h}(\mathbf{x}_{k+1}, \mathbf{x}_k, \mathbf{u}_k) = 0$. With a slight abuse of notation, we set $\mathbf{x}_0 = \mathbf{x}_i$. Further, inequality constraints $\mathbf{g}(\mathbf{x}_k, \mathbf{u}_k) \leq 0$ are constructed based on \mathbb{C}_i and are only evaluated at the discrete time steps for \mathbf{x}_k and \mathbf{u}_k .

The resulting nonlinear program (NLP) per sample is given:

$$\begin{aligned} & \min_{\hat{\mathbf{y}}} && \mathbf{d}(\mathbf{y}_{\text{GT}}, \hat{\mathbf{y}}) \\ & \text{subject to} && \\ & \mathbf{h}(\mathbf{x}_{k+1}, \mathbf{x}_k, \mathbf{u}_k) = 0, && k = 0, 1, \dots, H-1 \\ & \mathbf{g}(\mathbf{x}_k, \mathbf{u}_k) \leq 0, && k = 0, 1, \dots, H-1 \\ & \mathbf{g}(\mathbf{x}_N) \leq 0, && \end{aligned} \quad (4)$$

with optimization vector $\hat{\mathbf{y}} = [\mathbf{x}_0^T, \mathbf{u}_0^T, \dots, \mathbf{x}_H^T, \mathbf{u}_{H-1}^T]^T$.

Remember that $\hat{\mathbf{y}}$ is a function of the parameters θ . Hence, the complete procedure must be differentiable in order to backpropagate the gradients. The next section will describe such an approach using a modified version of [8].

B. Explicit Equality Completion

Instead of directly regressing a trajectory of future states, it is a common practice [12] to output a sequence of control vectors and unroll a differentiable dynamics model. That is similar to the explicit completion procedure described by [8]. To be precise, the neural network \mathbf{N}_θ predicts a sequence of control vectors $\mathbf{u}_N \in \mathbb{R}^{n_u \times H-1}$. The sequence of states $\mathbf{x}_N \in \mathbb{R}^{n_x \times H}$ is then computed by iteratively applying equation (3), starting from the measured state \mathbf{x}_i , described by function $\mathbf{x}_N = \mathbf{f}_{\text{compl}}(\mathbf{u}_N, \mathbf{x}_i)$. The concatenation of both vectors results in $\bar{\mathbf{y}} = [\mathbf{u}_N^T, \mathbf{x}_N^T]^T$.

C. Inequality Correction

The completion process accounts for the equality constraints derived from the discretized robots system dynamics. To further consider the inequality constraints, a differentiable gradient-based correction procedure is applied [8]. Here, we take gradient steps along the manifold of states and controls satisfying the equality constraints towards a feasible region.

The gradient-based correction, described by function $\mathbf{f}_{\text{corr}}(\bar{\mathbf{y}})$, is initialized by $\bar{\mathbf{y}} = [\mathbf{u}_N^T, \mathbf{x}_N^T]^T$. The approach then

¹For ease of notation, we assume that the data's sample rate is equal to the used grid size for discretization here. In practice, we could also up or downsample the recorded data.

calculates the gradients of the inequality constraints w.r.t. the sequence of control vectors \mathbf{u}_N and takes n_{grad} steps along the gradients. With the learning rate $\gamma \in \mathbb{R}^+$ and abbreviating $\mathbf{f}_{\text{compl}}(\cdot) = \mathbf{f}_{\text{compl}}(\mathbf{u}_N, \mathbf{x}_i)$ formally the function is given by:

$$\mathbf{f}_{\text{corr}} \left(\begin{bmatrix} \mathbf{u}_N \\ \mathbf{f}_{\text{compl}}(\cdot) \end{bmatrix} \right) = \begin{bmatrix} \mathbf{u}_N - \gamma \Delta \mathbf{u}_N \\ \mathbf{f}_{\text{compl}}(\cdot) - \gamma \Delta \mathbf{f}_{\text{compl}}(\cdot) \end{bmatrix}, \quad (5)$$

with

$$\Delta \mathbf{u}_N = \nabla_{\mathbf{u}_N} \left\| \text{ReLU} \left(\alpha \odot \mathbf{g} \left(\begin{bmatrix} \mathbf{u}_N \\ \mathbf{f}_{\text{compl}}(\cdot) \end{bmatrix} \right) \right) \right\|_2^2, \quad (6)$$

and

$$\Delta \mathbf{f}_{\text{compl}}(\cdot) = \frac{\partial \mathbf{f}_{\text{compl}}(\cdot)}{\partial \mathbf{u}_N} \Delta \mathbf{u}_N. \quad (7)$$

Remember that \mathbf{g} denotes the inequality constraints, and ReLU describes a rectified linear unit function. $\alpha \in \mathbb{R}^a$ is a weighting vector. The result of the correction is the estimated solution $\hat{\mathbf{y}}$.

D. Training and Inference

As already noticed by [8], convergence of gradient-based methods is not guaranteed and depend on initialization. However, if initialized closed to an optimum these methods are highly effective. The softloss for training²

$$\mathcal{L}_{\text{soft}} = \mathbf{d}(\mathbf{y}_{\text{GT}}, \hat{\mathbf{y}}) + \lambda_g \|\text{ReLU}(\alpha \odot \mathbf{g}(\hat{\mathbf{y}}))\|_2 + \lambda_h \|\mathbf{h}(\hat{\mathbf{y}})\|_2, \quad (8)$$

enables a feasible or at least nearly feasible initial solution, such that the inequality correction converges during test time. $\lambda_g \in \mathbb{R}$ and $\lambda_h \in \mathbb{R}$ are weighting factors. Algorithm 1 summarizes the approach.

Algorithm 1 Deep Constraint Imitation Learning

- 1: **procedure** DCIL($\mathbf{e}_i, \mathbf{x}_i$)
 - 2: **compute** initial sequence of controls $\mathbf{u}_N = \mathbf{N}_\theta(\mathbf{e}_i)$
 - 3: **complete** to $\bar{\mathbf{y}} = [\mathbf{u}_N^T, \mathbf{x}_N^T]^T$ with $\mathbf{f}_{\text{compl}}(\mathbf{u}_N, \mathbf{x}_i)$
 - 4: **correct** to estimated solution $\hat{\mathbf{y}} = \mathbf{f}_{\text{corr}}(\bar{\mathbf{y}})$ (function applied n_{grad} times)
 - 5: **if** train **then**
 - 6: **compute** loss (8) and **update** θ
 - 7: **else**
 - 8: **return** $\hat{\mathbf{y}}$
 - 9: **end if**
 - 10: **end procedure**
-

V. EXPERIMENTAL EVALUATION

This section evaluates the proposed approach in one mobile robot and one automated driving environment. This section addresses the following research questions: *Q1*: Does the approach improve the closed-loop performance of IL

²The loss in equation (8) described in the paper of [8] squares the norms of constraint violations. However, the official implementation (<https://github.com/locuslab/DC3>) uses the same loss as in this work. The authors of [8] verified that the mentioned implementation was used to generate the results of their paper. As later discussed in Section V-E, loss (8) also produced better results in our experiments.

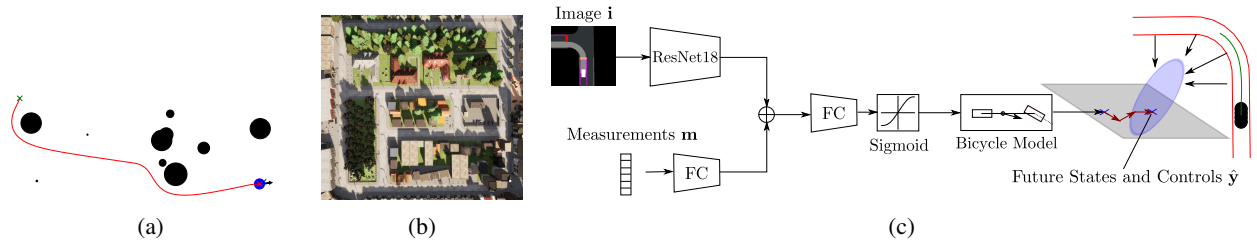


Fig. 2: (a) Mobile robot environment. Red visualizes one trajectory navigating from the green start point to the blue goal region while avoiding random obstacles (black). (b) Self-driving environment. (c) Network architecture in the SDE.

methods? *Q2*: How does the approach deal with incorrect constrain specifications?

Environments. The environments used for evaluation are visualized in Fig. 2a) and b).

Mobile Robot Environment (MRE): In the first environment data is collected by controlling a mobile robot with radius $r_{\text{robot}} = 1\text{m}$ using the Dynamic Window Approach [21]. The task during demonstrations is to navigate from a random start to a random goal location in the shortest time possible while avoiding collisions with circular shaped obstacles. Objects are randomly located with varying radii $r_c \in [0.1, 3]\text{m}$. The dataset contains 838 episodes (69638 samples), which were spitted in 83.3% training, and 8.3% validation and test each samples. This work evaluates closed-loop on another 76 *unseen* test episodes.

Self-Driving Environment (SDE): The second environment uses CARLA, a realistic automated driving simulator [22]. The CARLA Roach agent [23] collects training data. Further additive noise is applied to make the demonstrations more diverse, but sub-optimal. The dataset contains 120 episodes (174275 samples) from Town01, using the same ratios as in the MRE. We test on 25 random routes from a *different* environment (Town02) using the scenarios of the CARLA NoCrash-Challenge (Empty) [24] following the standardized evaluation protocol of the CALRA leaderboard. The SDV’s task it to follow the routes while avoiding collisions and obeying traffic lights.

Baselines. This work benchmarks against the following baselines. *IL*: The traditional imitation learning directly regresses a future state trajectory. *DKM*: An IL approach [12] predicting a sequence of control vectors bounded by a sigmoid layer. The controls and a dynamics model are then used to unroll a future state trajectory. *DKM \leq* : DKM with an additional gradient-based correction procedure only applied during test time, similar to a fallback layer as in [14]. *SL*: The same approach as IL trained using the softloss $\mathcal{L}_{\text{soft}}$. That is similar to [9], but here the soft constraints are not computed in image space.

Metrics. The MRE uses the following metrics: *Goal Reaching Rate (GRR)*: Rate of reached goals. *Collision Rate (CR)*: Rate of collision-prone episodes. *Time*: Percentage of the agents completion time relative to the expert trajectory. This metric measures efficiency. *Kinematic Constraint Violations (KCV)*: Summed number of constraint violations (tolerance: $1e-4$) of velocity, angular velocity, acceleration, and angular acceleration.

The SDE uses the metrics of the official CARLA Leaderboard Benchmark. We focus on closed-loop metrics as open-loop metrics can be a poor indicator to the actual task performance of robot policies [20].

A. Implementation

The method is agnostic and not restricted to the specific design choices made here.

State and Controls. A robot-centric coordinate system describes the state. *MRE*: The state \mathbf{x} is defined by a 2-D position with $x, y \in \mathbb{R}$ and $\phi \in SO(2)$. The robot controls \mathbf{u} are described by a forward $v \in \mathbb{R}$ and rotational velocity $\omega \in \mathbb{R}$. During testing, the flatness property of the unicycle model is used to compute the control values based on the predicted state trajectory. One could also directly use the predicted control values in a MPC formulation. However, the IL baseline only predicts a state sequence. Therefore, for a fair comparison, DCIL uses the same control strategy.

SDE: State \mathbf{x} and controls \mathbf{u} are the same as in [12]. During the evaluation, two PID controllers track the predicted state sequence of all methods.

Inputs. In both environments the input of the neural network \mathbf{e}_i constitutes of an image $\mathbf{i} \in \mathbb{R}^{a \times b \times c}$ with resolution $\text{res} \in \mathbb{R}$ and a measurement vector $\mathbf{m} \in \mathbb{R}^{n_m}$.

MRE: The robot centric image has dimensions $a = b = 128\text{px}$ with $\text{res} = 10 \frac{\text{px}}{\text{m}}$. One channel $c = 1$ describes the binary occupancy information. \mathbf{m} contains the current v and ω . It is further described by the distance $d_{\text{goal}} \in \mathbb{R}$ and heading $\theta_{\text{goal}} \in SO(2)$ w.r.t. the goal point. The dimension of the estimated control and state sequence $\hat{\mathbf{y}}$, is defined by $H = 10$ with time interval $\Delta t = 0.3\text{s}$.

SDE: The image has dimensions $a = b = 192\text{px}$ with $\text{res} = 5 \frac{\text{px}}{\text{m}}$. The SDV is centered in all images at 40px above the bottom. Different semantic classes from the work of [23] are color coded using the RGB channels with $c = 3$ as visualized in 2c). \mathbf{m} contains the current 2-D velocity $\mathbf{v} \in \mathbb{R}^2$, acceleration $\mathbf{a} \in \mathbb{R}^2$, and current speed limit v_{max} . We set $H = 20$ and $\Delta t = 0.2\text{s}$.

Constraints. *MRE*: For the dynamics, which constitute the equality constraints, we use a unicycle model as in [25]. This work applies box constraints such that $v \in [-0.5, 1] \frac{\text{m}}{\text{s}}$, $\omega \in [-0.70, 0.70] \frac{\text{rad}}{\text{s}}$, $a \in [-0.2, 0.2] \frac{\text{m}}{\text{s}^2}$, $\dot{\omega} \in [-0.70, 0.70] \frac{\text{rad}}{\text{s}^2}$. The acceleration a and angular acceleration $\dot{\omega}$ are computed from finite differences. For collision avoidance, we compute euclidean distances d_{obs} between the robot and the obstacles, as both footprints are circles. Then the state of every predicted

time step is constrained such that $d_{\text{obst}} > r_{\text{robot}} + r_c + 0.1$ m. As the algorithm requires a fixed number of constraints, it uses the three closest obstacles in the front half level of the robot.

SDE: In the CARLA experiments, this work uses the extended bicycle model for the dynamics (3) as [12] with vehicle sizes of a Lincoln MKZ. We bound the velocity by $v_{\text{max}} = 8.33 \frac{\text{m}}{\text{s}}$. Further the control accelerations are constrained by $a \in [-8, 4] \frac{\text{m}}{\text{s}^2}$, and the control steering angles by $\delta \in [-1, 1]$ rad. For collision avoidance, this work constructs a polyline-based driving corridor as in [26] using the high-level route. Four circles approximate the vehicle footprint. At every gradient step, the algorithm estimates the shortest distance to the left and right lane boundary for every predicted time step k and every circle. Further logical constraints for traffic lights are imposed. If a traffic light is yellow or red, it constructs a stopping line in front of the vehicle. Otherwise, due to the required fixed number of constraints, this line is created far away so that it does not influence the correction step. For the stopping line and the driving corridor, the inequality constraints are described as point-line distances. For a visual example of the constraints refer to Fig. 2c).

Loss. *MRE*: Let subscript $\hat{\cdot}$ define the estimated state or control of $\hat{\mathbf{y}}$. Based on related work [12], losses are:

$$\begin{aligned} \mathbf{d}(\mathbf{y}_{\text{GT}}, \hat{\mathbf{y}}) &= \sum_{k=1}^H (\hat{x}_k - x_{k,\text{GT}})^2 + (\hat{y}_k - y_{k,\text{GT}})^2 \\ &+ \left(\cos(\hat{\phi}_k) - \cos(\phi_{k,\text{GT}}) \right)^2 + \left(\sin(\hat{\phi}_k) - \sin(\phi_{k,\text{GT}}) \right)^2. \end{aligned} \quad (9)$$

SDE: The work of [27] showed that it is also beneficial to use an regularization term in the form of an inverse dynamics model. This work follows this approach:

$$\begin{aligned} \mathbf{d}(\mathbf{y}_{\text{GT}}, \hat{\mathbf{y}}) &= \sum_{k=1}^H |\hat{x}_k - x_{k,\text{GT}}| + |\hat{y}_k - y_{k,\text{GT}}| \\ &+ |\cos(\hat{\phi}_k) - \cos(\phi_{k,\text{GT}})| + |\sin(\hat{\phi}_k) - \sin(\phi_{k,\text{GT}})| \\ &+ \lambda_u \left(\sum_{k=0}^{H-1} |\cos(\hat{\phi}_k) - \cos(\phi_{k,\text{INV}})| + |\sin(\hat{\phi}_k) - \sin(\phi_{k,\text{INV}})| \right. \\ &\quad \left. + \sum_{k=0}^{H-2} |\hat{a}_k - a_{k,\text{INV}}| \right) \end{aligned} \quad (10)$$

Here λ_u describes a weighting factor and index INV denotes signals estimated with inverse model [27].

Network Architecture and Parameters. *MRE*: The binary image \mathbf{i} is encoded by a LeNet [28] outputting a latent vector, which is concatenated with the measurement vector \mathbf{m} . Afterwards, the result is processed by the same 2-layer fully connected network (FCN) of [8]. The predicted control sequence is bounded by a sigmoid layer and passed to the completion and correction step. In both environments we choose the hyperparameters by grid searches. In MRE we choose: $\lambda_g = \lambda_h = 0.5$, $\alpha = \mathbf{1}$.

SDE: A ResNet18 [29] first encodes the RGB image \mathbf{i}

TABLE I: Closed-loop performance of all methods using unseen test scenarios the in mobile robot environment.

Methode	GRR	CR	Time	KCV
	[%], \uparrow	[%], \downarrow	[%], \downarrow	[% (#)], \downarrow
IL	100	3.94	106	7.20 (4600)
SL	92	6.57	117	2.06 (1317)
DCIL	100	0.00	105	0.12 (89)

and the measurement vector \mathbf{m} is encoded by a 1-layer FCN. The concatenation of both encodings is passed to the previously described 2-layer FCN. Fig. 2c) visualizes the network architecture. In SDE we choose: $\lambda_g = 5$, $\lambda_h = 5$, $\lambda_u = 1$. Vector α is defined by weighting factors for the different inequality constraints. Collision are weighted by factor $\alpha_c = 1$, stopping line violations by $\alpha_s = 2$ and bounds on kinematic values by $\alpha_k = 1$. Both experiments use $\gamma = 1e - 3$ and $n_{\text{grad}} = 5$. For a fair comparison we ran grid searches for all baselines.

B. MRE Results

To answer *Q1*, DCIL is compared against the described baselines. Table I visualizes the results. DCIL outperforms all baselines in all metrics and it is the only one, which reaches all goals and without any collisions. Moreover, compared to the normal IL baseline, the number of kinematic constraint violations is reduced by a factor of 51.69. A qualitative comparison in an exemplary scenario is visualized in Fig. 3a). DCIL is the only method planning a collision-free trajectory. This can be attributed to the correction procedure acting as a safety layer.

C. SDE Results

Again considering question *Q1*, refer to the quantitative comparison of Table II. Note that IL++ describes the same approach as IL, but uses a PID-controller which takes more time to tune, such that the evaluation favors IL++. However, DCIL performs best in the different metrics of the CARLA leaderboard. We observed that the other baselines (IL, DKM, SL) often plan trajectories, that divert the from its route or onto the opposite. That is explained by their behavior under distribution shifts. Fig. 3c) illustrates such an qualitative result using the IL method. The closed-loop metrics in Table II also underline the described failures of the baselines.

Let us consider question *Q2*. In the CARLA experiments, the bicycle model [12] is an approximation of the real vehicle dynamics. However, it serves as an *inductive bias*, simplifying the learning process, and enhancing generalization capabilities, as shown by the closed-loop results in Table II. To further answer *Q2*, this work conducts another experiment, in which the SDV is spawned onto the wrong lane as illustrated in Fig. 4b). Note that the SDV never encountered such a situation during training, and hence this initial state is entirely outside the manifold of the training data. That situation could occur due to disturbances during driving or because a parked vehicle blocks the lane. Here, some hard constraint methods as [3] provide no solution at

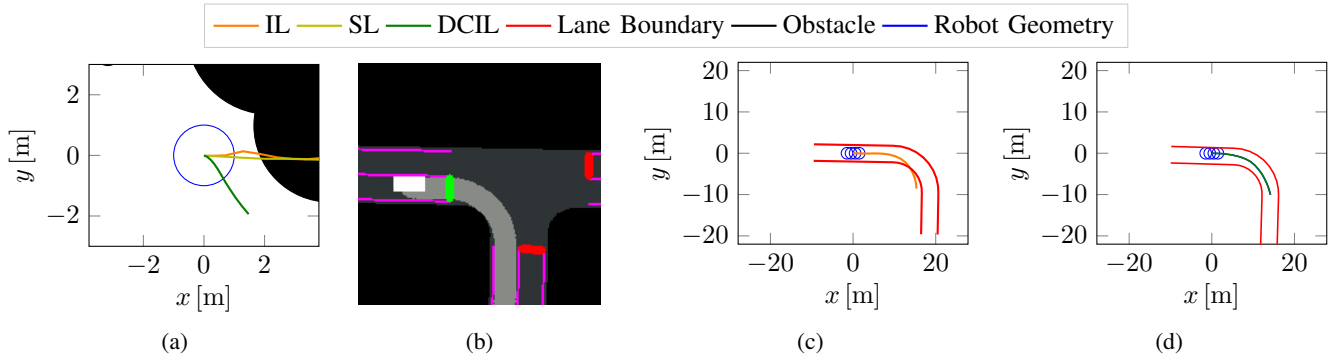


Fig. 3: Qualitative comparison. (a) Open-loop prediction results of the different methods in the MRE. (b) BEV input image of the neural network representing in CARLA. White pixels denote the SDV, black static obstacles, dark grey the road, light grey the route, and violet lane markings. Traffic lights are visualized by green or red color. The image is rotated by 90 degree (c) Constraint plot of the IL agent during closed-loop control. (d) DCIL during closed-loop control.

TABLE II: Closed-loop performance of all methods using unseen test routes in Town02 from CARLA-NoCrash.

Methode	Success rate	Driving score	Route completion	Infraction penalty	Collision layout	Red light infraction	Agent blocked	Outside of lane	Wrong lane
	[%], \uparrow	[%], \uparrow	[%], \uparrow	[%], \uparrow	[/Km], \downarrow	[/Km], \downarrow	[/Km], \downarrow	[/Km], \downarrow	[/Km], \downarrow
IL	36	50.18	44	95.65	1.44	0.42	525.00	0.06	5.73
IL++	52	62.33	80	98.84	5.70	0.27	94.28	3.39	9.41
DKM	76	76.69	92	98.94	1.40	0.11	6.90	0.00	8.85
DKM \leq	76	87.66	96	98.94	0.94	0.13	3.26	0.15	0.09
SL	92	96.09	100	100.00	0.35	0.00	0.00	0.00	0.21
DCIL	96	97.40	100	98.94	0.22	0.18	0.00	0.00	0.00

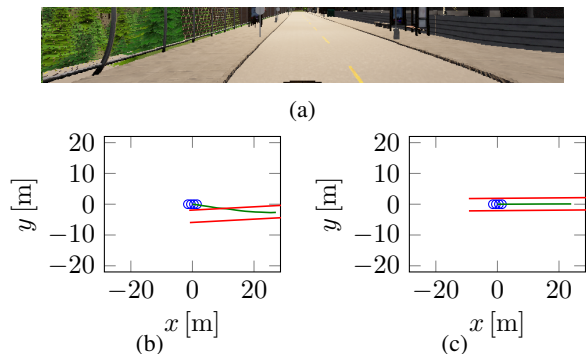


Fig. 4: Experiment, in which the SDV is spawned in an infeasible OOD state. (a) Camera image of the scene. (b) Initial infeasible configuration at $t = 0$ s. (c) DCIL successfully leads the vehicle back to the right lane at $t = 4$ s.

all, as the initial state is already infeasible. However, DCIL is robust w.r.t. incorrect specifications and leads the vehicle back onto the right lane, as visualized in Fig. 4c).

D. Runtime

The experiments use a AMD Ryzen 9 5900X and a Nvidia RTX 3090. Our non-optimized python implementation takes on average 20.02 ms in the MRE and 119.22 ms in the SDE.

E. Discussion, Limitations and Future Work

This section discusses the limitations of the presented work and gives an outlook on possible future directions. First, many active constraints make the loss landscape challenging to optimize and the procedure can be trapped in

local minima. We observed that results of SL and DCIL get worse (SDE: both methods' driving score drops by about 15%) using the described squared loss of [8]. That can be explained by the fact that the squared loss is more sensitive to outliers and harder to optimize during training, especially in the SDE. Hence we decided to use the non-squared loss of the official implementation [8] as mentioned in Section IV-D. Second, the paper at hand assumes that the constraints are known precisely. However, in many applications, the constraints are often uncertain (e.g., multi-modal predictions of human behavior with corresponding probabilities). The approach should be extended considering these in future work. Further staying in the multi-agent setting, we could also use the method presented for a constrained joint planning for multiple agents imitating human behavior. Third, due to the recent progress in perception, this work assumes a given object-based environment model. As our approach is fully differentiable, the proposed method could also be integrated into multi-task learning approaches as [30], which jointly train perception, prediction, planning, and control.

VI. CONCLUSION

This work proposed an approach combining ideas from IL with direct methods from optimal control for robot motion planning and control. It accounts for constraints using a differentiable completion and correction procedure. The experiments revealed that our approach proposed work outperforms multiple baselines in one mobile robot and one automated driving environment and can deal with infeasible initial states.

REFERENCES

- [1] J. Betts, "Practical methods for optimal control and estimation using nonlinear programming, 2nd ed.," 01 2010.
- [2] C. Rösmann, F. Hoffmann, and T. Bertram, "Kinodynamic trajectory optimization and control for car-like robots," in *2017 IEEE/RSJ International Conference on Intelligent Robots and Systems (IROS)*, 2017, pp. 5681–5686.
- [3] C. Rösmann, A. Makarow, and T. Bertram, "Online motion planning based on nonlinear model predictive control with non-euclidean rotation groups," in *2021 European Control Conference (ECC)*, 2021, pp. 1583–1590.
- [4] C. Diehl, A. Makarow, C. Rösmann, and T. Bertram, "Time-optimal nonlinear model predictive control for radar-based automated parking," *IFAC-PapersOnLine*, vol. 55, no. 14, pp. 34–39, 2022, 11th IFAC Symposium on Intelligent Autonomous Vehicles IAV 2022.
- [5] W. B. Knox, A. Allievi, H. Banzhaf, F. Schmitt, and P. Stone, "Reward (mis)design for autonomous driving," 2021, arxiv:2104.13906.
- [6] C. Diehl, T. Sievernich, M. Krüger, F. Hoffmann, and T. Bertram, "Umbrella: Uncertainty-aware model-based offline reinforcement learning leveraging planning," in *Advances in Neural Information Processing Systems, Machine Learning for Autonomous Driving Workshop*, 2021.
- [7] S. Ross, G. Gordon, and D. Bagnell, "A reduction of imitation learning and structured prediction to no-regret online learning," in *Proceedings of the Fourteenth International Conference on Artificial Intelligence and Statistics*, ser. Proceedings of Machine Learning Research, vol. 15. Fort Lauderdale, FL, USA: PMLR, 11–13 Apr 2011, pp. 627–635.
- [8] P. L. Donti, D. Rolnick, and J. Z. Kolter, "DC3: A learning method for optimization with hard constraints," in *International Conference on Learning Representations (ICLR)*, 2021.
- [9] M. Bansal, A. Krizhevsky, and A. Ogale, "Chauffeurnet: Learning to drive by imitating the best and synthesizing the worst," in *Proceedings of Robotics: Science and Systems*, June 2019.
- [10] Y. Nandwani, A. Pathak, Mausam, and P. Singla, "A primal dual formulation for deep learning with constraints," in *Advances in Neural Information Processing Systems*, vol. 32, 2019.
- [11] W. Zeng, W. Luo, S. Suo, A. Sadat, B. Yang, S. Casas, and R. Urtaun, "End-to-end interpretable neural motion planner," in *IEEE/CVF Conference on Computer Vision and Pattern Recognition (CVPR)*, 2019.
- [12] H. Cui, T. Nguyen, F.-C. Chou, T.-H. Lin, J. Schneider, D. Bradley, and N. Djuric, "Deep kinematic models for kinematically feasible vehicle trajectory predictions," in *2020 IEEE International Conference on Robotics and Automation (ICRA)*, 2020, pp. 10 563–10 569.
- [13] T. Phan-Minh *et al.*, "Driving in real life with inverse reinforcement learning," 2022, arxiv:2206.03004.
- [14] M. Vitelli *et al.*, "SafetyNet: Safe planning for real-world self-driving vehicles using machine-learned policies," in *2022 International Conference on Robotics and Automation (ICRA)*, 2022, pp. 897–904.
- [15] J. Zhou, R. Wang, X. Liu, Y. Jiang, S. Jiang, J. Tao, J. Miao, and S. Song, "Exploring imitation learning for autonomous driving with feedback synthesizer and differentiable rasterization," in *2021 IEEE/RSJ International Conference on Intelligent Robots and Systems (IROS)*, 2021, pp. 1450–1457.
- [16] B. Amos and J. Z. Kolter, "OptNet: Differentiable optimization as a layer in neural networks," in *Proceedings of the 34th International Conference on Machine Learning*, vol. 70, 2017, pp. 136–145.
- [17] A. Agrawal, B. Amos, S. Barratt, S. Boyd, S. Diamond, and J. Z. Kolter, "Differentiable convex optimization layers," in *Advances in Neural Information Processing Systems*, vol. 32, 2019.
- [18] M. Brosowsky, F. Keck, O. Dünkel, and M. Zöllner, "Sample-specific output constraints for neural networks," *Proceedings of the AAAI Conference on Artificial Intelligence*, vol. 35, no. 8, pp. 6812–6821, May 2021.
- [19] K. Leung and M. Pavone, "Semi-supervised trajectory-feedback controller synthesis for signal temporal logic specifications," *CoRR*, 2022, arxiv:2202.01997.
- [20] W. Xiao, T.-H. Wang, M. Chahine, A. Amini, R. Hasani, and D. Rus, "Differentiable control barrier functions for vision-based end-to-end autonomous driving," *CoRR*, 2022, arxiv:2203.02401.
- [21] D. Fox, W. Burgard, and S. Thrun, "The dynamic window approach to collision avoidance," *IEEE Robotics and Automation Magazine*, vol. 4, no. 1, pp. 23–33, 1997.
- [22] A. Dosovitskiy, G. Ros, F. Codevilla, A. Lopez, and V. Koltun, "CARLA: An open urban driving simulator," in *Proceedings of the Conference on Robot Learning*, 2017, pp. 1–16.
- [23] Z. Zhang, A. Liniger, D. Dai, F. Yu, and L. Van Gool, "End-to-end urban driving by imitating a reinforcement learning coach," in *Proceedings of the IEEE/CVF International Conference on Computer Vision (ICCV)*, October 2021, pp. 15 222–15 232.
- [24] F. Codevilla, S. Eder, A. M. Lopez, and A. Gaidon, "Exploring the limitations of behavior cloning for autonomous driving," in *IEEE/CVF International Conference on Computer Vision*, 2019, pp. 9328–9337.
- [25] T.-C. Lee, K.-T. Song, C.-H. Lee, and C.-C. Teng, "Tracking control of unicycle-modeled mobile robots using a saturation feedback controller," *IEEE Transactions on Control Systems Technology*, vol. 9, no. 2, pp. 305–318, 2001.
- [26] J. Ziegler, P. Bender, T. Dang, and C. Stiller, "Trajectory planning for bertha — a local, continuous method," in *2014 IEEE Intelligent Vehicles Symposium Proceedings*, 2014, pp. 450–457.
- [27] F. Janjoš, M. Dolgov, and J. M. Zöllner, "Self-supervised action-space prediction for automated driving," in *2021 IEEE Intelligent Vehicles Symposium (IV)*, 2021, pp. 200–207.
- [28] Y. Lecun, L. Bottou, Y. Bengio, and P. Haffner, "Gradient-based learning applied to document recognition," *Proceedings of the IEEE*, vol. 86, no. 11, pp. 2278–2324, 1998.
- [29] K. He, X. Zhang, S. Ren, and J. Sun, "Deep residual learning for image recognition," in *Proceedings of the IEEE conference on computer vision and pattern recognition (CVPR)*, 2016, pp. 770–778.
- [30] D. Chen and P. Krähenbühl, "Learning from all vehicles," in *Proceedings of the IEEE/CVF Conference on Computer Vision and Pattern Recognition (CVPR)*, June 2022, pp. 17 222–17 231.